Orientation as a key parameter in the valence-subband-structure engineering of quantum wells

G. Shechter, L. D. Shvartsman, and J. E. Golub
Racah Institute of Physics, The Hebrew University of Jerusalem, Jerusalem, Israel
(Received 14 September 1994)

The quantum well spectra orientation dependence of cubic semiconductors is studied through a simplification of the valence-subband dispersion relation, applicable for the three symmetrically oriented (perpendicular to the lattice symmetry axes) quantum wells. The semianalytical treatment which is based on the Kohn-Luttinger formalism, incorporates the effect of strain, and is generalized for gapless semiconductors as well as for III-V compounds. The rectangular and hexagonal in-plane symmetries of the ⟨011⟩ and ⟨111⟩ films, respectively, are studied by calculating the full subband dispersion in these orientations for GaAs, InAs, Ge, HgTe, and α-Sn. The rectangular symmetry of ⟨011⟩ films can result in spectral saddle points at $\boldsymbol{k}_{\|} = \mathbf{0}$. Orientation is also found to be an important parameter in tailoring surface state branches in gapless semiconductors.

I. INTRODUCTION

Valence-band-structure engineering in cubic semiconductor strained quantum wells (QW's) is an important arena in which to develop new applications in such electronic devices as low-threshold lasers[1] and high-mobility hole channel[2] transistors. The results of a qualitative analysis[3] and recent experiments[4,5] have demonstrated that the crystallographic orientation of the QW plays a crucial role in determining the subband structure, and can be an important degree of freedom in designing devices. The role of orientation stems mainly from the corrugation of the bulk energy spectrum. A number of analytical[6–12] and numerical[13–15] calculations of the valence-subband structure, based on the Kohn-Luttinger Hamiltonian,[16] were devoted to ⟨001⟩-oriented layers. Such studies are facilitated by the square in-plane symmetry of these layers. An accurate description of the valence-band structure in differently oriented heterostructures has until now required the use of numerical methods,[17,18] making the design process rather tedious.

In this paper, we present semianalytical calculations of the valence-subband structure of ⟨011⟩- and ⟨111⟩-oriented quantum wells of cubic semiconductors. Instead of the perturbative approach used in Ref. 19 to find only the masses of subbands at $\boldsymbol{k}_{\|} = \mathbf{0}$, we show an algebraic derivation, applicable for ⟨001⟩, ⟨011⟩, and ⟨111⟩ layers, which simplifies the dispersion relation drastically and enables us to find the full subband structure semianalytically. In contrast to our paper[20] on ⟨011⟩ layers, the present calculations incorporate the effect of strain, and are generalized for gapless semiconductors as well as for III-V compounds. Also, the dispersion relations and effective masses near $\boldsymbol{k}_{\|} = \mathbf{0}$ are given in a much more compact form. Note that the square and the hexagonal symmetries of the ⟨001⟩ and ⟨111⟩ films, respectively, promises isotropic mass, where the rectangular symmetry of ⟨011⟩ films can result in spectral saddle points at $\boldsymbol{k}_{\|} = \mathbf{0}$.

In Sec. II, we explain why film orientation is dominant in determining the valence-subband structure in QW's, and discuss the general theoretical approach to be used. The Hamiltonian and its accompanying boundary conditions are described in more details in Sec. III, where simplified dispersion relations for the ⟨011⟩- and ⟨111⟩-oriented QW's are derived, and the effect of strain on the subband structure is incorporated. In this section, we also give an analytical expression for the effective mass tensor, show numerically the full subband dispersion for the representative materials GaAs, InAs, Ge, HgTe, and α-Sn, and discuss experimental implications. Finally, in Sec. IV, we show how orientation can also be an important parameter in tailoring surface state branches in gapless semiconductors, making use of the valence-band anisotropy.

II. THEORETICAL APPROACH

Before beginning a detailed analysis of the valence-subband structure in generally oriented QW's, it should first be understood why orientation gives an important degree of freedom in tailoring this structure. Then it is important to clarify the limitations of the theoretical method.

A. Statement of the problem

As first shown in Ref. 6, two factors are principally responsible for the unusual in-plane dispersion in these systems: (1) corrugation of the isoenergetic surfaces of the bulk materials; and (2) nonconservation of the z projection of the total momentum by $J=3/2$ holes upon reflection from the heterointerface. In practice, the warping of the bulk bands is the dominant factor with the result that crystallographic orientation plays a key role—and offers an interesting degree of freedom—in determining

0163-1829/95/51(16)/10857(12)/$06.00

the in-plane dispersion of the QW. We next demonstrate this point by considering quasiclassical quantization in the ⟨011⟩ and ⟨111⟩ layers.[7] In the quasiclassical limit, we find the two-dimensional ⟨011⟩ bands by considering the bulk bands,

$$E^{(1,2)}(\boldsymbol{k}) = Ak^2 \pm \{B^2k^4 + C^2[k_x^2k_y^2 + k_x^2k_z^2 + (k_z^2 - k_y^2)/4]\}^{1/2} \quad (1)$$

under the condition $k_z = n\pi/d$, where d is the layer thickness. Here A, B, and C are valence-band constants connected with the Luttinger parameters γ_1, γ_2, γ_3 as in Ref. 21. n is the quasiclassical subband index and Eq. (1) is written in the ⟨011⟩ film coordinate system here defined by the ⟨100⟩, ⟨01$\bar{1}$⟩, and ⟨011⟩ directions. Similarly, the ⟨111⟩ two-dimensional bands are found by writing the bulk dispersion in the ⟨111⟩ film coordinates here defined by the ⟨1$\bar{1}$0⟩, ⟨11$\bar{2}$⟩, and ⟨111⟩ directions:

$$E^{(1,2)}(\boldsymbol{k}) = Ak^2 \pm \{B^2k^4 + C^2/3 \times [k_z^4 + 3/4(k_y^2 + k_x^2)^2 + 2^{1/2}k_zk_y(k_y^2 - 3k_x^2)]\}^{1/2}, \quad (2)$$

and by taking $k_z = n\pi/d$.

Figure 1 shows the two-dimensional (2D) heavy hole dispersion which results from Eqs. (1) and (2). Evidentially, the dispersion is extremely different for ⟨100⟩ and ⟨01$\bar{1}$⟩ directions in the plane of the ⟨011⟩ film. In particular, the figure shows the existence of saddle point dispersion in a number of subbands, though the quasiclassical approach does not make clear in which band the saddle point behavior will occur. The detailed behavior is obtained in the quantum mechanical treatment given in Sec. III.

B. Validity of the model

We work in the effective mass/envelope function approximation.[16] The results, therefore, do not apply to the very thinnest films. We also adopt the flat band approximation, and neglect the spin splitting, which occurs in the energy spectrum of the QW's, due to the inversion asymmetry of the microscopic crystal potential.[22] The characteristic confinement energies in which we are interested are of the order of 50 meV, while the depth of the well and spin-orbit splitting of the valence-band are of several hundred meV. For this reason, we use the infinite well model and neglect any coupling with the spin-orbit split valence-subband, keeping in mind that only low states are occupied. Numerical results for higher subbands can be considered as estimates.

Unlike in ⟨001⟩ QW's, in more general orientations the heavy hole (HH) band is coupled with the light hole (LH) and split-off (SO) bands by the kinetic part of the Hamiltonian even at $\boldsymbol{k}_{\|} = \boldsymbol{0}$. Still, for heavy (light) subbands, the ⟨011⟩ and ⟨111⟩ spectra at $\boldsymbol{k}_{\|} = \boldsymbol{0}$, is found under the infinite well model to depend only on the bulk heavy (light) hole mass in the direction perpendicular to the layer, which is effected by this kinetic coupling.

The neglect of the SO band coupling becomes even more troublesome in the case of a strained QW. The use of lattice-mismatched materials introduces a shear - strain coupling in the bulk matrix Hamiltonian between the LH and SO bands,[12,15] and causes the bulk HH-LH splitting to vary nonlinearly with strain. To second order in strain terms, this splitting is given by $2\xi(1+\xi/\Delta)$, where Δ is the spin-orbit splitting, and 2ξ is the splitting found after neglecting the strain-dependent coupling between the LH and SO bands. Unlike in ⟨001⟩, the use of ⟨011⟩- and ⟨111⟩-oriented lattice-mismatched materials introduces a shear-strain coupling between the HH and SO bands, as well as between the LH and SO bands. The shear-strain SO interaction also induces a change of the order of ξ/Δ in the LH and HH bulk effective masses. Thus, the ratio ξ/Δ gives a measure of the error in the LH and HH solutions incurred by neglecting this coupling. Justifying the neglect of the shear-strain coupling with the SO band is the fact that for typical QW's like

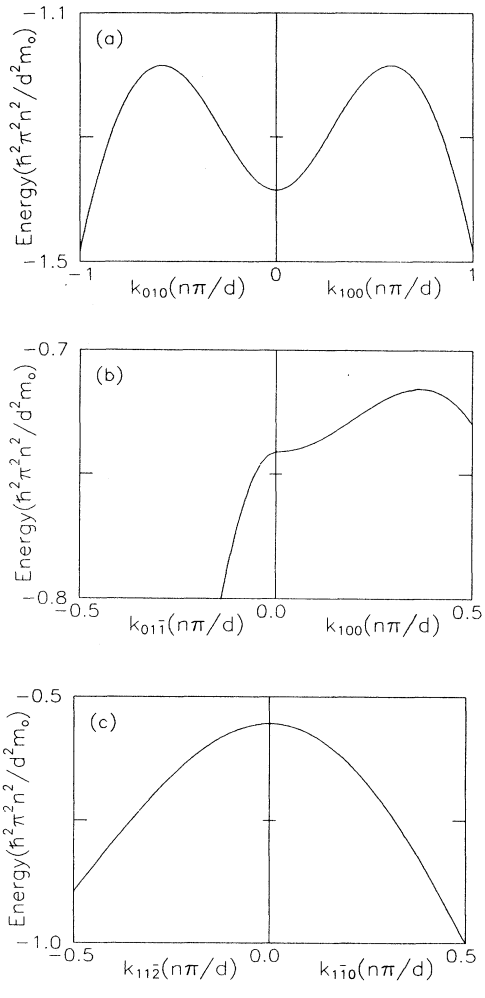

FIG. 1. Quasiclassical dispersion of GaAs heavy hole subbands. The curves give the limiting dispersion for the case $n \gg 1$ and are obtained from the bulk dispersion under the conditions (a) $k_{\langle 001\rangle} = n\pi/d$, (b) $k_{\langle 011\rangle} = n\pi/d$, and (c) $k_{\langle 111\rangle} = n\pi/d$.

that of a ⟨011⟩-oriented $In_{0.2}Ga_{0.8}As$ layer strained by an AlAs barrier the ratio ξ/Δ is 11%, making the error incurred acceptable. Note that compressive strain only serves to further separate the HH and SO bands, and reduces the influence of the kinetic coupling between them.

III. SEMIANALYTIC SOLUTION FOR THE VALENCE-SUBBAND STRUCTURE IN ⟨011⟩- AND ⟨111⟩-ORIENTED QUANTUM WELLS

In this section, a simplified representation of the dispersion relation is derived for ⟨011⟩- and ⟨111⟩-oriented strain induced QW's. Effective masses of subbands at $\boldsymbol{k}_{\|} = \mathbf{0}$ for the unstrained layers are also given. The derivation is applicable also for ⟨001⟩ QW's for which analogous simplified expressions for the dispersion relation and effective masses are given in Refs. 7 and 9.

A. Dispersion and effective masses for the unstrained QW

Reference 7 gives the 4×4 Luttinger Hamiltonian for the Γ_8 point in ⟨001⟩ coordinates. The Hamiltonian has the form

$$H = \hbar^2/m_0 \begin{pmatrix} L & S & N & 0 \\ S^* & M & 0 & N \\ N^* & 0 & M & -S \\ 0 & N^* & -S^* & L \end{pmatrix}, \tag{3}$$

where in ⟨001⟩ coordinates

$$L = -\frac{\gamma_1+\gamma_2}{2}k_{||}^2 + \left(\gamma_2 - \frac{\gamma_1}{2}\right)k_z^2, \tag{4a}$$

$$M = -\frac{\gamma_2-\gamma_1}{2}k_{||}^2 + \left(\gamma_2 + \frac{\gamma_1}{2}\right)k_z^2, \tag{4b}$$

$$N = \frac{\sqrt{3}}{2}\gamma_2(k_y^2 - k_x^2) + \sqrt{3}\gamma_3 i k_x k_y, \tag{4c}$$

$$S = \sqrt{3}\gamma_3 i(k_x - ik_y)k_z \ . \tag{4d}$$

For other orientations, it is convenient to write the Hamiltonian in a system of coordinates k_θ, k_ϕ, k_r, where $\hat{r}$ is perpendicular to the plane of the layer. This is achieved by the transformation :

$$\begin{pmatrix} k_x \\ k_y \\ k_z \end{pmatrix} = T_{\theta,\phi}\begin{pmatrix} k_\theta \\ k_\phi \\ k_r \end{pmatrix}, \tag{5}$$

where

$$T_{\theta,\phi} \equiv \begin{pmatrix} \cos\theta\cos\phi & -\sin\phi & \sin\theta\cos\phi \\ \cos\theta\sin\phi & \cos\phi & \sin\theta\sin\phi \\ -\sin\theta & 0 & \cos\theta \end{pmatrix} . \tag{6}$$

θ and ϕ are defined by the representation of $\hat{r}$ in the ⟨001⟩ coordinates. In particular, for ⟨001⟩ coordinates $\theta = \phi = 0$, for ⟨011⟩ coordinates $\theta = \pi/4, \phi = \pi/2$ and for ⟨111⟩ coordinates $\theta = \arccos(1/\sqrt{3}), \phi = \pi/4$.

We first discuss the solutions of the wave equation in the bulk. The components of the Bloch vector $\mathbf{k}$ are good quantum numbers, and the envelope function can be taken to be of the form $\underline{F}(\boldsymbol{r}) = \underline{f}e^{i\boldsymbol{k}\cdot\boldsymbol{r}}$ where $\underline{f} = (f_1, f_2, f_3, f_4)$ is an eigenvector of the Luttinger kinetic matrix (3). The secular equation gives the well known hole dispersion relation,

$$E = (L+M)/2 \pm [(L-M)^2/4 + NN^* + SS^*]^{1/2} \ . \tag{7}$$

For III-V compounds the plus sign refers to heavy holes and the minus sign to light holes. The same Hamiltonian (3) also describes the band structure of gapless semiconductors since they have the same Γ_8 symmetry. There, instead of a light hole band one has an electron band, which also has the p-type symmetry. Below, for the case of gapless semiconductors, the band with the index "l" is the electron band. For example, in Eq. (7) for gapless semiconductors, the reference to light and heavy holes is exchanged and so the plus sign refers to electrons and the minus sign to holes. For a given energy and $\boldsymbol{k}_{\|}$, Eq. (7) is satisfied by four eigenvalues k_r. Each eigenvalue is twofold degenerate, since the Hamiltonian is invariant with respect to both space inversion and time reversal, due to our neglect of linear terms in k in Eq. (3). We denote the eigenvalues as $k_{j\pm} = \kappa_{j0} \pm \kappa_j; j = h, l$. For small values of $\boldsymbol{k}_{\|}, k_{h\pm}$ correspond to the heavy hole branch, while $k_{l\pm}$ correspond to the light one. However, because of the corrugation of isoenergetic surfaces, this correspondence does not occur for larger values of $\boldsymbol{k}_{\|}$. In any system of coordinates, $\kappa_{j0} = 0$ at $\boldsymbol{k}_{\|} = \mathbf{0}$, and $k_{j-} = -k_{j+}$. In ⟨001⟩ and ⟨011⟩ coordinates we further have $\kappa_{j0} = 0$ for $\boldsymbol{k}_{\|} \neq \mathbf{0}$, unlike in ⟨111⟩ coordinates where $\kappa_{j0} \neq 0$ for $\boldsymbol{k}_{\|} \neq \mathbf{0}$.

In the case of the QW, the potential $V(r)$ breaks translation symmetry along $\hat{r}$; however, k_θ and k_ϕ remain good quantum numbers. Using the approach of Refs. 2, 6, 7, 9, and 10, a hole state in the well may be found as that linear combination of the eight bulk wave functions, which vanishes at the well boundaries. The requirement for existence of such a linear combination is given in Eq. (8) and generates the QW dispersion relation:

$$\det \begin{pmatrix} S_{h_+} & -N_{h_+} & S_{h_-} & -N_{h_-} & S_{l_+} & -N_{l_+} & S_{l_-} & -N_{l_-} \\ -L_{h_+} & 0 & -L_{h_-} & 0 & -L_{l_+} & 0 & -L_{l_-} & 0 \\ 0 & L_{h_+} & 0 & L_{h_-} & 0 & L_{l_+} & 0 & L_{l_-} \\ N^*_{h_+} & S^*_{h_+} & N^*_{h_-} & S^*_{h_-} & N^*_{l_+} & S^*_{l_+} & N^*_{l_-} & S^*_{l_-} \\ S_{h_+}e_{h_+} & -N_{h_+}e_{h_+} & S_{h_-}e_{h_-} & -N_{h_-}e_{h_-} & S_{l_+}e_{l_+} & -N_{l_+}e_{l_+} & S_{l_-}e_{l_-} & -N_{l_-}e_{l_-} \\ -L_{h_+}e_{h_+} & 0 & -L_{h_-}e_{h_-} & 0 & -L_{l_+}e_{l_+} & 0 & -L_{l_-}e_{l_-} & 0 \\ 0 & L_{h_+}e_{h_+} & 0 & L_{h_-}e_{h_-} & 0 & L_{l_+}e_{l_+} & 0 & L_{l_-}e_{l_-} \\ N^*_{h_+}e_{h_+} & S^*_{h_+}e_{h_+} & N^*_{h_-}e_{h_-} & S^*_{h_-}e_{h_-} & N^*_{l_+}e_{l_+} & S^*_{l_+}e_{l_+} & N^*_{l_-}e_{l_-} & S^*_{l_-}e_{l_-} \end{pmatrix} = 0 \ , \tag{8}$$

where

$$L_{j\pm}, N_{j\pm}, S_{j\pm} = L, N, S(\boldsymbol{k}_{\|}, k_{j\pm}),$$
$$e_{j\pm} = \exp(ik_{j\pm}d) \quad j = h, l\ . \tag{9}$$

For $\boldsymbol{k}_{\|} = \mathbf{0}$, the dispersion relation reduces to $\sin(k_h d)\sin(k_l d) = 0$. This simplified relation reflects the fact that at $\boldsymbol{k}_{\|} = \mathbf{0}$ the HH and LH bulk bands are decoupled and the QW spectra is calculated as in the nondegenerate case. Subbands are designated light and heavy according to $k_l d = n\pi$ and $k_h d = n\pi$, respectively, for $\boldsymbol{k}_{\|} = \mathbf{0}$. The index n denotes the subband number. In contrast to $\langle 001\rangle$-grown films, N and S in Eq. (4) do not vanish at $\boldsymbol{k}_{\|} = \mathbf{0}$ for differently oriented films. This coupling between bulk HH and LH bands affects the solutions for wave functions at $\boldsymbol{k}_{\|} = \mathbf{0}$. Thus, the complexity involved in applying a perturbative approach increases substantially for different film orientations.

Equation (8) can be written in the form

$$aR^2 + (x - a - c)R + c = 0, \tag{10}$$

where

$$R = \frac{(e_{h+} - e_{l-})(e_{l+} - e_{h-})}{(e_{h+} - e_{h-})(e_{l+} - e_{l-})}\ , \tag{11a}$$

$$\begin{aligned} a &= G_{k_{h+},k_{h-}} G_{k_{l+},k_{l-}}, \\ c &= G_{k_{h+},k_{l-}} G_{k_{l+},k_{h-}}, \\ x &= G_{k_{h+},k_{l+}} G_{k_{h-},k_{l-}}, \end{aligned} \tag{11b}$$

and G_{k_1,k_2} is the determinant of the 4×4 matrix, built from the four eigenvectors of the Luttinger kinetic matrix corresponding to the eigenvalues k_1 and k_2. G_{k_1,k_2} can be written as

$$G_{k_1,k_2} \equiv \det \begin{pmatrix} L_{k_1}S_{k_2} - L_{k_2}S_{k_1} & L_{k_2}N_{k_1} - L_{k_1}N_{k_2} \\ L_{k_1}N^*_{k_2} - L_{k_2}N^*_{k_1} & L_{k_1}S^*_{k_2} - L_{k_2}S^*_{k_1} \end{pmatrix}. \tag{12}$$

Recalling that k_1 and k_2 satisfy Eq. (7), we find

$$\begin{aligned} G_{k_1,k_2} = L_{k_1}L_{k_2} \times [&(L_{k_1} - L_{k_2})(M_{k_1} - M_{k_2}) \\ &-(N_{k_1} - N_{k_2})(N^*_{k_1} - N^*_{k_2}) \\ &-(S_{k_1} - S_{k_2})(S^*_{k_1} - S^*_{k_2})]. \end{aligned} \tag{13}$$

From Eqs. (10), (11), and (13) we can discard from now on the term $L_{k_1}L_{k_2}$ in G_{k_1,k_2} without changing the dispersion relation. From Eqs. (4)–(6), we get

$$\begin{aligned} G_{k_1,k_2} = (k_1 - k_2)^2[&R_0^{(\theta,\phi)} + R_1^{(\theta,\phi)}(k_1 + k_2) \\ &+R_2^{(\theta,\phi)}(k_1 + k_2)^2], \end{aligned} \tag{14}$$

where

$$\begin{aligned} R_0^{(\theta,\phi)} \equiv\ & k_\theta^2[3\gamma_3^2 + 12(\gamma_3^2 - \gamma_2^2)\sin^2\theta\cos^2\theta(\sin^2\phi\cos^2\phi - 1)] + k_\phi^2[3\gamma_3^2 - 12(\gamma_3^2 - \gamma_2^2)\sin^2\theta\sin^2\phi\cos^2\phi] \\ &+k_\theta k_\phi[12(\gamma_3^2 - \gamma_2^2)\sin^2\theta\cos\theta\sin\phi\cos\phi(\cos^2\phi - \sin^2\phi)], \end{aligned} \tag{15}$$

$$R_1^{(\theta,\phi)} \equiv 6k_\theta(\gamma_3^2 - \gamma_2^2)\sin\theta\cos\theta[1 + 2\sin^2\theta(\sin^2\phi\cos^2\phi - 1)] + 6k_\phi(\gamma_3^2 - \gamma_2^2)\sin^3\theta\sin\phi\cos\phi(\cos^2\phi - \sin^2\phi), \tag{16}$$

$$R_2^{(\theta,\phi)} \equiv \gamma_2^2 - \gamma_1^2/4 + 3(\gamma_3^2 - \gamma_2^2)\sin^2\theta(\cos^2\theta + \sin^2\theta\sin^2\phi\cos^2\phi)\ . \tag{17}$$

Note that

$$R_2^{(\theta,\phi)} = -\nu_h^{(\theta,\phi)}\nu_l^{(\theta,\phi)}/4\ , \tag{18}$$

where ν_l^{-1} and ν_h^{-1} are the bulk light and heavy masses perpendicular to the layer in units of m_0.

The complexity of Eq. (10) enables us to find the subband structure only by massive numerical calculations. Obviously, the dispersion relation becomes drastically simpler whenever the two roots for R satisfying Eq. (10) coincide. Substituting Eq. (14) in Eq. (10), we find that the two roots for R satisfying Eq. (10) coincide whenever

$$R_1^{(\theta,\phi)} + R_2^{(\theta,\phi)}\sum_{i=1}^{4} k_{r_i} = 0\ . \tag{19}$$

The three symmetric system of coordinates are the only ones for which $R_1^{(\theta,\phi)}$ and $k_{h+} + k_{h-} + k_{l+} + k_{l-}$ are zero for any $\boldsymbol{k}_{\|}$, satisfying Eq. (19). Using this relation, we write the dispersion relations of the symmetrically oriented QW's in the following compact form:

$$\begin{aligned} &\frac{\cos(2\kappa_0 d) - \cos(\kappa_h d + \kappa_l d)}{\sin(\kappa_h d)\sin(\kappa_l d)} \\ &\quad = \frac{[(\kappa_h + \kappa_l)^2 - 4\kappa_0^2][R_0 - \nu_h\nu_l(\kappa_h - \kappa_l)^2/4]}{2\kappa_h\kappa_l(R_0 - \nu_h\nu_l\kappa_0^2)}\ . \end{aligned} \tag{20}$$

Here, $\kappa_0 = \kappa_{h0} = -\kappa_{l0}$. R_0 is defined in Eq. (15) and for the symmetric system of coordinates is given explicitly as

$$R_0^{\langle 001\rangle} = 3\gamma_3^2 k_{\|}^2, \tag{21}$$

$$R_0^{\langle 011\rangle} = 3\gamma_2^2 k_\theta^2 + 3\gamma_3^2 k_\phi^2, \tag{22}$$

$$R_0^{\langle 111\rangle} = (\gamma_3^2 + 2\gamma_2^2)k_{\|}^2\ . \tag{23}$$

The $\nu_j(\theta,\phi)$ are found directly from the bulk dispersion Eq. (7):

$$\nu_j^{\langle 001\rangle} = -\gamma_1 \pm 2\gamma_2, \tag{24}$$

$$\nu_j^{\langle 011\rangle} = -\gamma_1 \pm (\gamma_2^2 + 3\gamma_3^2)^{1/2}\ \mathrm{sign}(\gamma_1^2 - \gamma_2^2 - 3\gamma_3^2), \tag{25}$$

$$\nu_j^{\langle 111\rangle} = -\gamma_1 \pm 2\gamma_3\ . \tag{26}$$

Here, the upper (lower) sign corresponds to heavy (light) subbands. The hexagonal symmetry in the $\langle 111\rangle$ layer is thus hidden inside the $k_{j\pm}$. Henceforth, we drop the notations θ, ϕ when writing ν_j.

We next discuss the behavior near zone center. For small $k_{||}$, the $\langle 011\rangle$ dispersion has the form

$$E^{\langle 011\rangle}_{j,(n)}(\boldsymbol{k}_{||}) = \hbar^2 n^2 \pi^2 \nu_j/(2m_0 d^2) - (\hbar^2/2)(k_\theta^2/m^{(n)}_{\theta,j} + k_\phi^2/m^{(n)}_{\phi,j}) \ . \quad (27)$$

The form of Eq. (27) is consistent with the rectangular symmetry. Here, m_θ and m_ϕ denote the effective masses along k_θ and k_ϕ, which for $\langle 011\rangle$ orientation are given by $\langle 01\bar{1}\rangle$ and $\langle \bar{1}00\rangle$, respectively [see Eqs. (5), (6)]. The effective masses may be derived by series expansion of the dispersion relation Eq. (20) near $\boldsymbol{k}_{||} = \boldsymbol{0}$. We adjust the signs of the masses so that bulk, isotropic hole masses are positive [see the minus sign in Eq. (27)]. Under this convention, bulk isotropic electron masses of gapless semiconductors are negative. For $\langle 011\rangle$-oriented QW heavy subbands, we find

$$\frac{m_0}{m^{\langle 011\rangle}_{h,\theta,(n)}} = \frac{-12\gamma_2^2\sqrt{\nu_h}\sqrt{\nu_l}}{\gamma_2^2+3\gamma_3^2}\frac{\cos(n\pi\sqrt{\nu_h}/\sqrt{\nu_l})+(-1)^{n+1}}{n\pi\sin(n\pi\sqrt{\nu_h}/\sqrt{\nu_l})} - \frac{6(\gamma_2^2-\gamma_3^2)}{(\gamma_2^2+3\gamma_3^2)^{1/2}}\ \mathrm{sign}(\nu_h-\nu_l)-\nu_h, \quad (28a)$$

$$\frac{m_0}{m^{\langle 011\rangle}_{h,\phi,(n)}} = \frac{-12\gamma_3^2\sqrt{\nu_h}\sqrt{\nu_l}}{\gamma_2^2+3\gamma_3^2}\frac{\cos(n\pi\sqrt{\nu_h}/\sqrt{\nu_l})+(-1)^{n+1}}{n\pi\sin(n\pi\sqrt{\nu_h}/\sqrt{\nu_l})} + \frac{3(\gamma_2^2-\gamma_3^2)}{(\gamma_2^2+3\gamma_3^2)^{1/2}}\ \mathrm{sign}(\nu_h-\nu_l)-\nu_h \ . \quad (28b)$$

Masses of light subbands are found by exchanging the indices l and h in Eq. (28). For $\langle 111\rangle$-oriented QW's, we have $m_{\theta,j,(n)} = m_{\phi,j,(n)} = m_{j,(n)}$ as dictated for any analytic curvature near $\boldsymbol{k}_{||} = \boldsymbol{0}$, by the hexagonal in-plane symmetry.

$$\frac{m_0}{m^{\langle 111\rangle}_{h,(n)}} = \frac{(2\gamma_2^2+\gamma_3^2)}{-\gamma_3^2/(\sqrt{\nu_h}\sqrt{\nu_l})}\frac{\cos(n\pi\sqrt{\nu_h}/\sqrt{\nu_l})+(-1)^{n+1}}{n\pi\sin(n\pi\sqrt{\nu_h}/\sqrt{\nu_l})} + \gamma_1 + \frac{8\gamma_2^2}{\nu_l-\nu_h} \ . \quad (29)$$

Masses of light subbands are found by exchanging the indices l and h in Eq. (29). By taking $n \to \infty$, we return to the quasiclassical approximation shown in Fig. 1. We present the effective masses for GaAs, InAs, Ge, HgTe, and α-Sn films calculated from Eqs. (28) and (29) in Table I. The table caption gives the values of the relevant Luttinger parameters.

We will now discuss the dependence of the subband structure on the QW orientation. By numerical solutions of Eq. (20), we present the subband structure of different materials in $\langle 011\rangle$ and $\langle 111\rangle$ layers, (see Figs. 2 and 3). Comparing the results with the $\langle 001\rangle$ layers subband structure[6,9] shows that changing the orientation results in a transition of the first excited subband from a negative mass at $\boldsymbol{k}_{||} = \boldsymbol{0}$ through a saddle point (see Fig. 2) to a positive mass (see Fig. 3). Changing the orientation results also in a different order of subbands at $\boldsymbol{k}_{||} = \boldsymbol{0}$ [see Figs. 2(c)] and 3(c)), as can be easily seen from the equality,

$$E_{j,(n)}(\boldsymbol{k}_{||} = \boldsymbol{0}) = \hbar^2 n^2 \pi^2 \nu_j/(2m_0 d^2) \ . \quad (30)$$

The negative sign of the HH1 subband hole effective mass in gapless semiconductors [see Figs. 2(d),(e) and 3(d),(e)] is not caused by corrugation of the bulk dispersion and is evidentially independent of the film orientation. It is a result of the total momentum nonconservation by the electrons and the holes upon reflection from the heterointerface. A deeper explanation for the electroniclike behavior of the HH1 subband, which makes the gap, induced by size quantization, to be the minimal energy distance between the HH1 and HH2 subbands, is given in Sec. IV. Unlike in $\langle 001\rangle$ and $\langle 011\rangle$ layers, in $\langle 111\rangle$ layers this gap corresponds to $\boldsymbol{k}_{||} = \boldsymbol{0}$. The value of this gap is a crucial parameter in a lot of kinetic and optical phenomena. For α-Sn it is equal to 17.3,[9] 18.2, and 13.3 in $\langle 001\rangle$-, $\langle 011\rangle$-, and $\langle 111\rangle$-oriented layers, respectively, in units of $\hbar^2/(m_0 d^2)$. The intersections between subbands in Figs. 2(c) and (e) are in agreement with the isotropic approximation,[23] which allows subbands with the same j to intersect when their n numbers are of different parities, while subbands with different j may intersect when their n's are of the same parity.

TABLE I. Effective masses at $k_{||} = 0$, in units of m_0, for GaAs, InAs, Ge, HgTe, and α-Sn, $\langle 011\rangle$ and $\langle 111\rangle$ layers.

Material	Subband index	Type	$m^{\langle 011\rangle}_{\langle 100\rangle}$	$m^{\langle 011\rangle}_{\langle 01\bar{1}\rangle}$	$m^{\langle 111\rangle}$
GaAs[a]	1	h	0.129	0.092	0.103
"	2	h	-0.205	0.260	0.417
"	1	l	0.064	0.112	0.126
InAs[b]	1	h	0.045	0.039	0.041
"	2	h	-0.258	0.228	0.352
"	1	l	0.016	0.030	0.059
Ge[c]	1	h	0.072	0.057	0.062
"	2	h	-0.134	0.382	0.698
"	1	l	0.037	0.053	0.054
HgTe[d]	1	h	-0.051	-0.062	-0.057
"	2	h	-0.353	0.247	0.383
"	1	l	-0.046	-0.036	-0.037
α-Sn[e]	1	h	-0.040	-0.101	-0.065
"	2	h	-0.093	0.052	0.066
"	1	l	-0.068	-0.025	-0.025

[a](From Ref. 28) : $\gamma_1 = 7.63, \gamma_2 = 2.43, \gamma_3 = 3.26$.
[b](From Ref. 21) : $\gamma_1 = 19.67, \gamma_2 = 8.37, \gamma_3 = 9.29$.
[c](From Ref. 7) : $\gamma_1 = 13.00, \gamma_2 = 4.45, \gamma_3 = 5.35$.
[d](From Ref. 21) : $\gamma_1 = -14.80, \gamma_2 = -9.00, \gamma_3 = -8.20$.
[e](From Ref. 28) : $\gamma_1 = -15.14, \gamma_2 = -11.40, \gamma_3 = -8.02$.

B. Strained-layer quantum wells

We now consider the case of an internal strain, built into the QW, due to lattice mismatch between the well and barrier materials grown along the same crystallographic direction. For demonstration we consider $\langle 011\rangle$

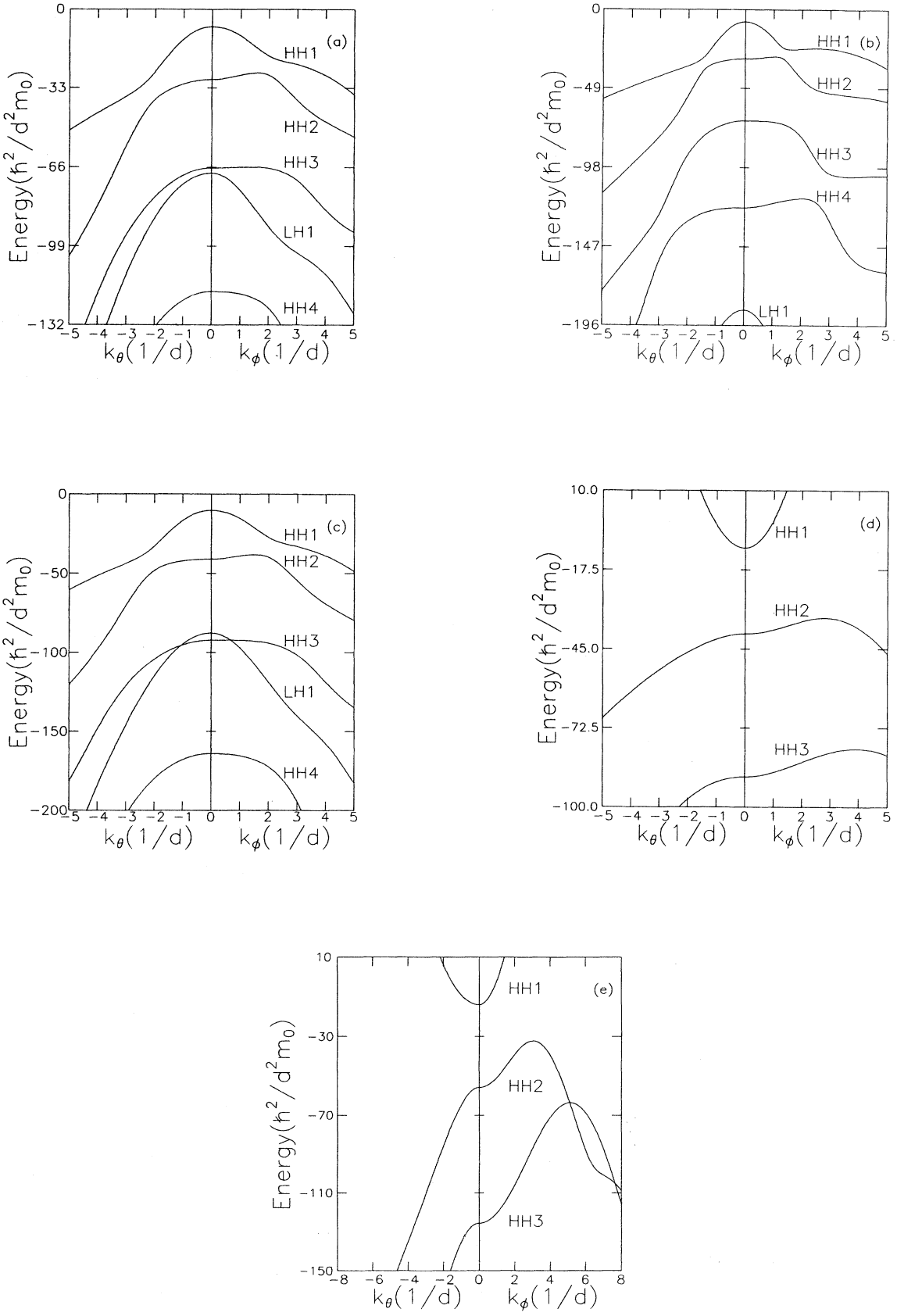

FIG. 2. In-plane dispersion for ⟨011⟩ QW's; (a) GaAs, (b) InAs, (c) Ge, (d) HgTe, (e) α-Sn.

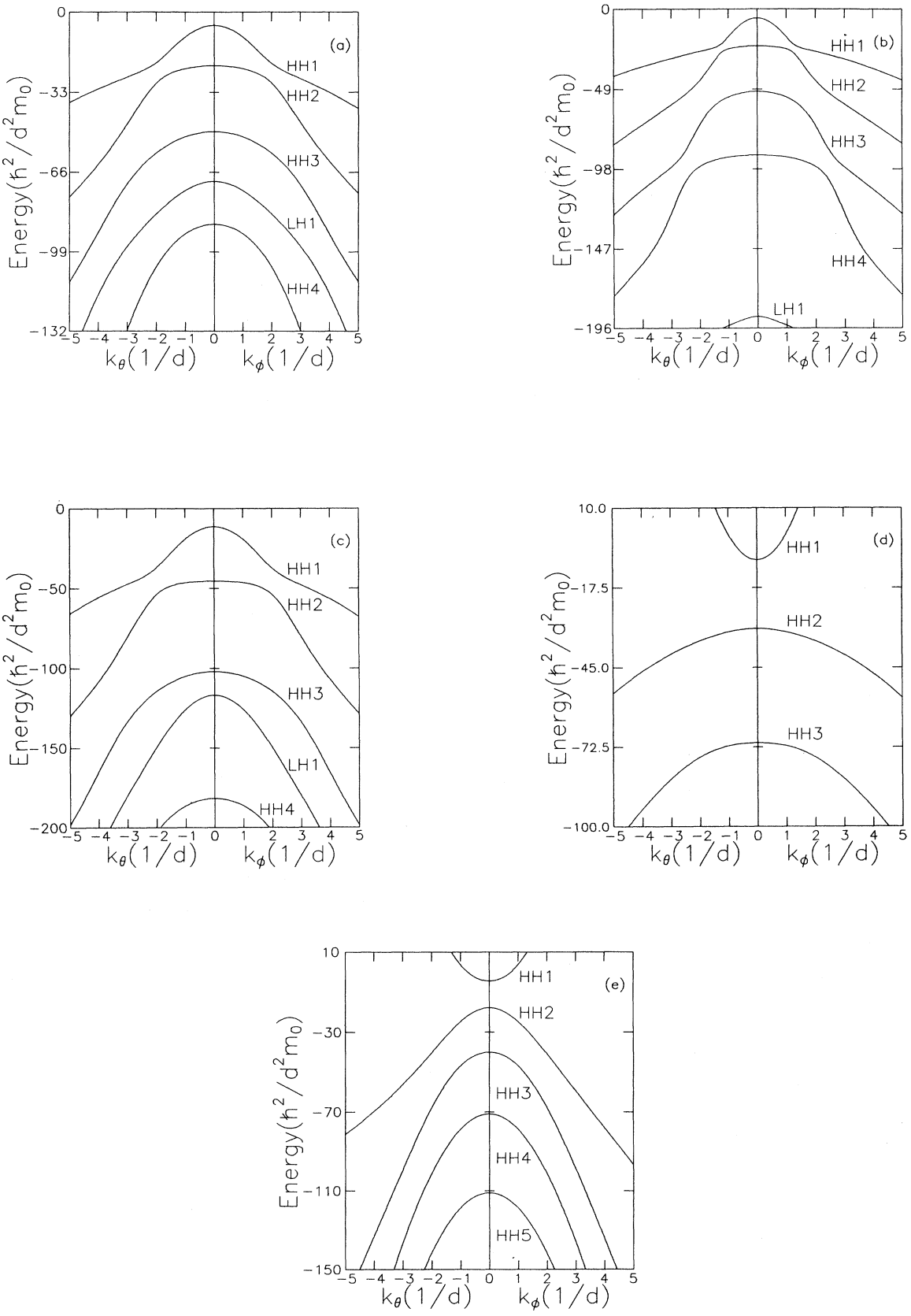

FIG. 3. In-plane dispersion for ⟨111⟩ QW's; (a) GaAs, (b) InAs, (c) Ge, (d) HgTe, (e) α-Sn.

strained layers, although the treatment for ⟨111⟩ layers is essentially the same. In ⟨011⟩ coordinates, the strain tensor is given by

$$\epsilon = \begin{pmatrix} \epsilon_{||} & 0 & 0 \\ 0 & \epsilon_{||} & 0 \\ 0 & 0 & \epsilon_{\perp} \end{pmatrix} . \tag{31}$$

We limit ourself to the case of infinitely thick barrier materials, in which $\epsilon_{||}$ is just the fractional lattice mismatch[24] $(\Delta a_0/a_0)$. Here, Δa_0 is the difference of the lattice constants of the unstrained materials and a_0 is the average lattice constant. $\epsilon_{\perp}$ can be evaluated from the condition of zero stress in the direction perpendicular to the interface, denoted by σ_{rr}, which gives

$$\epsilon_{\perp} = \epsilon_{||} \frac{C_{44} - C_{11} - C_{12}}{C_{44} + C_{11} + C_{12}}, \tag{32}$$

where C_{11}, C_{12}, and C_{44} are elastic constants. Equation (32) is found after writing the strain tensor in ⟨001⟩ coordinates, and using the relation

$$\sigma_{rr} = \frac{\sigma_{z_0 z_0}}{2} + \frac{\sigma_{y_0 y_0}}{2} + \sigma_{y_0 z_0}, \tag{33}$$

where the index 0 stands for ⟨001⟩ coordinates. The strain tensor is given in ⟨001⟩ coordinates by

$$\epsilon_0 = \begin{pmatrix} \epsilon_{||} & 0 & 0 \\ 0 & (\epsilon_{||} + \epsilon_{\perp})/2 & (\epsilon_{\perp} - \epsilon_{||})/2 \\ 0 & (\epsilon_{\perp} - \epsilon_{||})/2 & (\epsilon_{||} + \epsilon_{\perp})/2 \end{pmatrix} . \tag{34}$$

The strained lattice looks unstrained from the "0s" system of coordinates, related to the ⟨001⟩ system of coordinates by

$$\mathbf{x}_{0s} = (1 + \epsilon_0)^{-1} \mathbf{x}_0 . \tag{35}$$

The 4×4 Luttinger Hamiltonian for the Γ_8 point containing deformation potentials has already been given in 0s coordinates.[25] While deformation potentials are not changed when writing the Hamiltonian in the film system of coordinates, the kinetic part of the Hamiltonian, written in the film coordinates, is found after replacing the representation of the wave vector in "0s" system of coordinates by its representation in the film system of coordinates, where it is denoted by $\boldsymbol{k}$. Note that

$$\boldsymbol{k}_{0s} = (1 + \epsilon_0) T_{\theta,\phi} \boldsymbol{k} . \tag{36}$$

Equation (36) shows the existence of terms involving the strain-wave-vector product. These terms increase the complexity of the equations and cannot be neglected in the case of tensile strained QW's. However, since in our case $\epsilon_{\theta,\phi} = \epsilon_{\theta,r} = \epsilon_{\phi,r} = 0$, this difficulty can be overcome by writing the Hamiltonian and obtaining the film dispersion relation using the variables $\boldsymbol{k}_s = (1 + \epsilon)\boldsymbol{k}$. We use the relation $\boldsymbol{k}_{0s} = T_{\theta,\phi} \boldsymbol{k}_s$. Therefore, the valence-subband dispersion can be calculated disregarding these terms, after proper scaling of E and $\boldsymbol{k}_{||}$. For the case of a compressively strained QW, these terms can be neglected. Repeating the approach of Sec. II A for the unstrained layers we learn from Eqs. (10–13), that the addition of deformation potential matrix elements in the strained-layer Hamiltonian does not effect the resulting dispersion relation Eq. (20) for the symmetrically oriented QW's. The effect of the strain on the subband structure is, of course, hidden in the altered dependence of the $k_{j\pm}$ on $\boldsymbol{k}_{||}$ and E.

The influence and magnitude of the strain on the hole spectrum vary with the film orientation. Only in ⟨001⟩ layers, does the applied strain result in a constant shift at $\boldsymbol{k}_{||} = \mathbf{0}$ of the heavy subbands relative to the light subbands: After neglect of terms involving the strain-wave-vector product in the Hamiltonian, the bulk dispersion of the light and heavy holes in the ⟨011⟩ direction is given by

$$E^{(1,2)}(k_r) = \tilde{a}\epsilon - \gamma_1 \hbar^2 k_r^2/(2m_0) \pm \left\{ \left[\frac{\tilde{b}}{2}(\epsilon_{||} - \epsilon_{\perp}) + \gamma_2 \hbar^2 k_r^2/(2m_0) \right]^2 + \left[\frac{\tilde{d}}{2}(\epsilon_{||} - \epsilon_{\perp}) + \sqrt{3}\gamma_3 \hbar^2 k_r^2/(2m_0) \right]^2 \right\}^{1/2} . \tag{37}$$

Here, $\tilde{a}, \tilde{b}$, and $\tilde{d}$ are deformation potentials. Since the ⟨011⟩ (like the ⟨111⟩) spectra at $\boldsymbol{k}_{||} = \mathbf{0}$ is found under the infinite well model to depend only on the bulk HH and LH dispersion in the direction perpendicular to the layer (see Sec. II), Eq. (37) shows that the applied strain does not result in a constant shift at $\boldsymbol{k}_{||} = \mathbf{0}$ of the heavy hole subbands relative to the light hole levels. That is in contrast to the situation in ⟨001⟩ layers, where the analog for Eq. (37) turns out not to couple k_r with deformation potentials.

Next, we consider the change of the valence-band structure of ⟨011⟩-oriented QW's, due to strain caused by lattice mismatch. In Fig. 4(a), we show the valence-subband structure of an AlAs/$In_{0.2}Ga_{0.8}As$/AlAs QW. For comparison, we present Fig. 4(b) in which the effect of lattice mismatch is not taken into account. The values of constants used in the calculations were obtained by linear interpolation from their values in GaAs and InAs given in Table II. We find a saddle point in the dispersion of the HH2 band in the unstrained layer. The deformation enlarges the repulsion between the first two heavy subbands with the result that the HH2 subband looses its saddle point at $\boldsymbol{k}_{||} = \mathbf{0}$. It is also interesting to see how the deformation changes the ordering of the HH4 and LH1 subbands at $\boldsymbol{k}_{||} = \mathbf{0}$.

C. Experimental implications

We next mention some experimental implications of the ⟨011⟩- oriented film dispersion laws presented in Fig. 2. In infrared absorption experiments, this dispersion should manifest itself as an interesting dependence of the absorption edge and line shape upon Fermi level. We consider intersubband transitions and search for tracks of saddle point dispersion in the joint density of states. Transitions between different type bands $(h \to l, l \to h)$ can manifest saddle point dispersion. When the pertur-

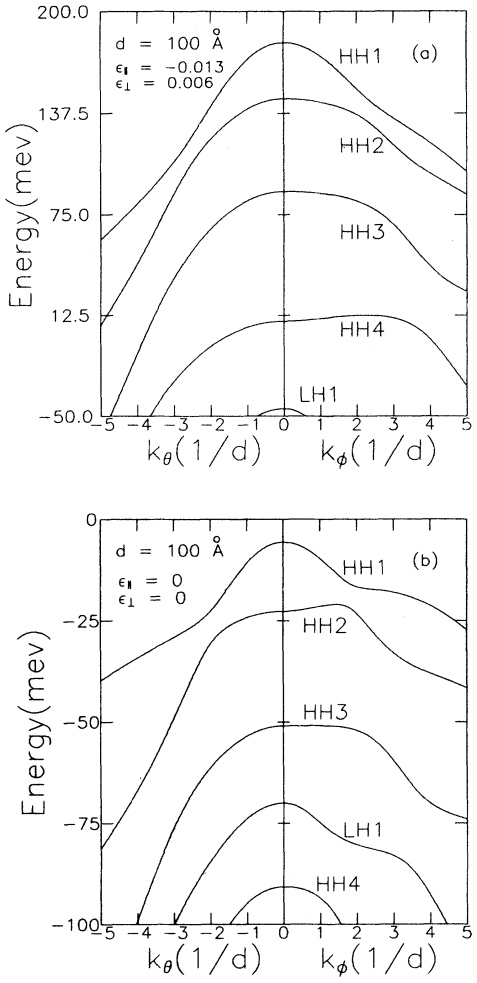

FIG. 4. In-plane dispersion for ⟨011⟩ $In_{0.2}Ga_{0.8}As/AlAs$ QW. In (b) the effect of lattice mismatch is not taken into account. The AlAs lattice constant is taken as (Ref. 21) 5.66 Å. The zero of energy is chosen as the valence-band edge of the unstrained $In_{0.2}Ga_{0.8}$ bulk.

bation of the Bloch functions at $\boldsymbol{k}_\parallel = \mathbf{0}$ is neglected, the p-type character of the valence-band[26] prevents transitions between different type bands of the infinite quantum well. We can prove that this statement is true for any orientation. For large $\boldsymbol{k}_\parallel$, these transitions are allowed and have been observed in experiments.[27] For transitions between like bands ($h \to h, l \to l$), there can be no saddle point dispersion. This new result follows from Eqs. (28). However, in the presence of strain, saddle point dispersion can result. We therefore consider next intersubband absorption in the presence of saddle point dispersion in the joint density of states. For illustration, consider first the case of transitions between parabolic subbands. In this simplest case, the absorption spectrum is narrow and independent of Fermi level. Hole transitions of III-V compounds in ⟨001⟩-oriented films give a less trivial behavior. There, the absorption spectrum broadens to a minimum lower energy as the Fermi level is increased due to the negative mass of the HH2 band. In the present case, we expect a narrow peak for low Fermi level. As the hole concentration is increased, the spectrum broadens to both higher and lower energies, due to the saddle point dispersion. At $\boldsymbol{k}_\parallel = \mathbf{0}$, we have a kink in the absorption spectrum due to the infinite joint density of states at the saddle point. The shape of the absorption curve thus carries information about the detailed band structure and includes a new feature characteristic of the saddle point. Alternatively, if the band structure is known, measurement of the infrared absorption spectrum permits a determination of the carrier concentration. This possibility does not exist in n-type films, where subbands are very nearly parabolic and parallel.

The valence-subband structure of ⟨111⟩-oriented film is given in Fig. 3 and is rather isotropic. Because of the small effective mass of the HH1 band in (a), (b), and (c), holes are heated very effectively by an electric field and can reach the HH2 band edge where they become heavier. At low temperatures this can lead to a range of negative differential conductivity which can be used in generating current oscillations.

The unusual dispersion of Figs. 2 and 3 may be manifested in cyclotron resonance experiments, where the holes are accelerated in spiral orbits about the axis of a magnetic field $\boldsymbol{H}$, applied in perpendicular to the layer. The angular rotation frequency is $\omega_c = \pm eH/m^*c$, where the energy dependent effective hole mass, m^* is given by

$$m^* = \frac{\hbar^2}{2\pi} \oint \frac{k_\parallel d\chi}{\partial E/\partial k_\parallel} , \tag{38}$$

and χ is the angle in plane of the layer. Considering the ⟨011⟩-oriented film of the III-V compounds, for low hole concentrations the dispersion dictates a single peak corresponding to the ground subband. Due to nonparabolicity, the cyclotron mass increases as the Fermi level is increased. When the Fermi level intersects the HH2 band, we expect an additional, doubly degenerate peak. As the Fermi level crosses the saddle point, the doubly degenerate peak disappears and is replaced by a single, nondegenerate peak as shown in Fig. 5. The resulting cyclotron

TABLE II. Material parameters for GaAs and InAs. All data are from Ref. 21.

Material	Lattice constant	Deformation potentials (eV)			Elastic constants (10^{11} dyn/cm^2)		
	(Å)	$\tilde{a}$	$\tilde{b}$	$\tilde{d}$	C_{11}	C_{12}	C_{44}
GaAs	5.65	−8.0	−1.9	−5.0	11.90	5.47	5.95
InAs	6.06	−6.0	−1.8	−3.6	8.33	4.53	3.96

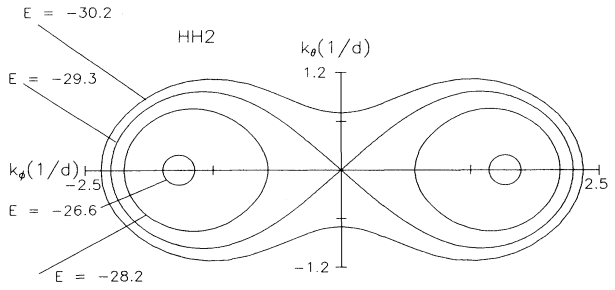

FIG. 5. Isoenergetic curves of the HH2 subband in ⟨011⟩-oriented GaAs QW. Energy is taken in units of $(\hbar^2/d^2m_0)$.

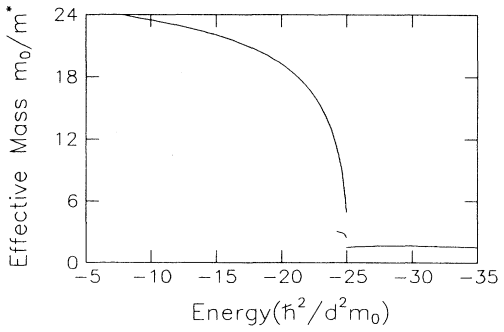

FIG. 7. Cyclotron mass of the ground heavy subband in ⟨011⟩ InAs QW.

mass is shown for GaAs in Fig. 6, in comparison to that of the ⟨111⟩-oriented film. The cyclotron mass of the ground subband of a ⟨011⟩-oriented InAs film is given in Fig. 7. The nonmonotonic dispersion of the subband along k_ϕ [see Fig. 2(b)] results in an additional, doubly degenerate peak for a small energy range.

IV. SURFACE STATES IN GAPLESS SEMICONDUCTORS

Additional branches of the electronic spectrum, attributable to the surface states, were found to exist in gapless semiconductors by D'yakonov and Khaetskii.[23] The wave function of an electron in such a state, a superposition of the electron states in the valence-band and in the conduction band, vanishes at the surface, has a maximum at a certain distance from it, and falls off exponentially deep into the crystal. These states were described within the context of the effective mass theory, and the isotropic approximation in which

$$\gamma = (2\gamma_2 + 3\gamma_3)/5 \tag{39}$$

replaces γ_2 and γ_3 in Eq. (4). As a result, the effective mass, which determines the motion along the surface in these states, was found to depend only on the mass ratio of the free electron and the free hole in the crystal. As

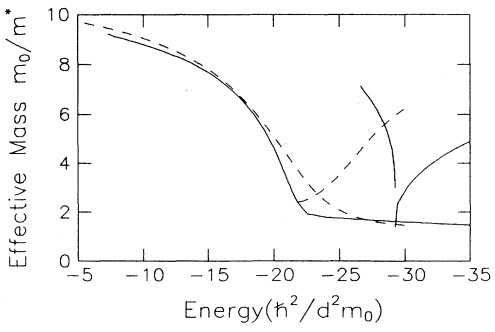

FIG. 6. Cyclotron mass of the first two heavy subbands in GaAs QW's. The solid lines denotes ⟨011⟩ orientation; dashed lines denotes ⟨111⟩ orientation.

will be shown, the simplification of the expression G_{k_1,k_2} made in Sec. III enables us to find surface states analytically without using the isotropic approximation. Doing so, we find that the surface orientation is an important parameter which, together with the Luttinger parameters determines whether surface states do exist in the crystal, and affects their 2D dispersion.

Suppose the crystal occupies a region $r > 0$, where r is the spatial coordinate perpendicular to the surface. The components of the wave vector along the surface k_θ and k_ϕ are good quantum numbers. A surface state is a superposition of the eight bulk solutions for the equation $H\Psi = E\Psi$ (see Sec. III), which satisfy the boundary condition $\Psi(r = 0) = 0$ and which decrease as $r \to \infty$. This latter condition constrains the surface state to be a superposition of only the bulk solutions satisfying

$$\mathrm{Im}(k_r) > 0 \ . \tag{40}$$

For specified values of $\boldsymbol{k}_\parallel$ and E there are four independent solutions of that kind, corresponding to the eigenvalues k_{h+} and k_{l+}. (Note that because the anisotropy of the bulk dispersion relation, k_{h+} and k_{l+} are not necessarily pure imaginary.) A superposition of these four solutions, which vanishes at $r = 0$, exists whenever

$$G_{k_{h+},k_{l+}} = 0 \ , \tag{41}$$

which together with Eq. (40) gives the surface states dispersion relation. The parabolic nature of the surface state dispersion in the plane of the surface is clearly reflected from Eqs. (13) and (41); therefore, we take $k_\parallel = 1$, leaving free only the angle between $\boldsymbol{k}_\parallel$ and k_ϕ, which we denote by χ. When the surface is perpendicular to one of the three axes of symmetry, Eq. (41) reduces to

$$R_0 - (\nu_h\nu_l/4)(k_{h+} + k_{l+})^2 = 0 \ . \tag{42}$$

Since $R_0 > 0$ (see Sec. III) and $\mathrm{Im}(k_{j+}) > 0$, it is clear that for III-V compounds, Eq. (42) has only a trivial solution; therefore, the surface states do not exist for these materials. Until now this result was known only under the isotropic approximation.

We now wish to convert the transcendental Eq. (42) into a clear dependence of E on χ. At this point, we

limit ourselves to ⟨001⟩- and ⟨011⟩-oriented surfaces and use the relation $k_{j-} = -k_{j+}$. Substituting the explicit form of the k_{j+}, given by $\sqrt{\alpha \pm \sqrt{\beta}}$, into Eq. (42), we find

$$\sqrt{\bar{a}E^2 + \bar{b}E + \bar{c}} + \bar{d}E + \bar{e} = 0 \ . \tag{43}$$

Here $\bar{a}, \bar{b} \ldots \bar{e}$ are well defined functions of γ_i and χ. Solutions of Eq. (43) for ⟨001⟩-oriented surfaces are given by

$$E_{1,2} = \frac{-3\gamma_1\gamma_2 \pm \sqrt{3}\sqrt{-\nu_h\nu_l}\sqrt{\gamma_2^2\cos^2(2\chi) + \gamma_3^2\sin^2(2\chi)}}{4\gamma_2} \tag{44}$$

under the restriction

$$\gamma_1^2 + 2\gamma_2^2 + 2\gamma_1 E_{1,2} > 0 \ . \tag{45}$$

The energy is given in units of $\hbar^2 k_{\|}^2/m_0$. For ⟨011⟩ surfaces, we find

$$E_{1,2} = \frac{-3\gamma_1[2\gamma_3^2 + (\gamma_2^2 - \gamma_3^2)\cos^2\chi]}{2(\gamma_2^2 + 3\gamma_3^2)} \pm \frac{2\sqrt{3}\gamma_3\sqrt{-\nu_h\nu_l}\sqrt{\gamma_2^2 - 3(\gamma_2^2 - \gamma_3^2)\cos^2\chi\sin^2\chi}}{2(\gamma_2^2 + 3\gamma_3^2)} \tag{46}$$

under the restriction

$$\gamma_1^2 + 2\gamma_2^2 + 3(\gamma_3^2 - \gamma_2^2)\sin^2\chi + 2\gamma_1 E_{1,2} > 0 \ . \tag{47}$$

Equations (44)–(47) enable a full classification of the 3D zones in γ_i space, for which zero, one, or two 2D surface states branches do exist. This full classification is beyond the scope of this paper. However, it is clear from Eq. (43) that for given γ_i and surface orientation, there exists exactly one surface state solution whenever

$$[\bar{d}(\chi)\,E_1 + \bar{e}][\bar{d}(\chi)\,E_2 + \bar{e}] < 0 \tag{48}$$

and zero or two solutions in the opposite case. For specified values of γ_i, the sign of the left part of Eq. (48) is surprisingly found to depend on the angle χ. This shows the existence of partial 2D branches of surface states, which cease to exist for specific values of χ. For example, in ⟨001⟩-oriented surfaces this phenomenon occurs when

$$(\gamma_2^2 - \gamma_1^2)(3\gamma_1^2\gamma_3^2 + \gamma_1^2\gamma_2^2 - 4\gamma_2^4) > 0 \ . \tag{49}$$

The disappearance of these branches occurs when they reach the 2D bulk band of the light (or of the heavy) holes (which corresponds to $k_r = 0$). At this angle, k_{l+} (or k_{h+}) equals zero and Ψ does not decrease as $r \to \infty$. Passing this angle, we continuously find a solution for Ψ, vanishing at $r = 0$, which is a superposition of bulk solutions corresponding to k_{l-} and k_{h+} (or to k_{h-} and k_{l+}). For known gapless semiconductors, this phenomenon does not occur in ⟨001⟩ and ⟨011⟩ surfaces where one branch—the electronlike surface states is found, corresponding to the plus sign in Eqs. (44) and (46). The same is found for the ⟨111⟩ surface after numerical investigation of Eq. (42). Calculated surface state branches for all three symmetrically oriented surfaces of HgTe and α-Sn are shown in Fig. 8.

We now go back to the QW problem and connect the electroniclike behavior of the HH1 subband in gapless semiconductors with the electronlike branch of surface states. We denote by CR the region in $(E, \boldsymbol{k}_{\|})$ space which corresponds to k_l and k_h having nonzero (positive) imaginary part. We denote these imaginary parts by I_l and I_h. Let us consider the limiting case $I_l d \gg 1, I_h d \gg 1$. Then, Eq. (20) coincides with Eq. (41) which describes the surface states branch. It follows that one of the subbands of the size quantization spectrum should go over at high $k_{\|}$ values into the electronlike surface states branch. This subband is found to be the HH1 subband when all the remaining subbands are not contained in CR.

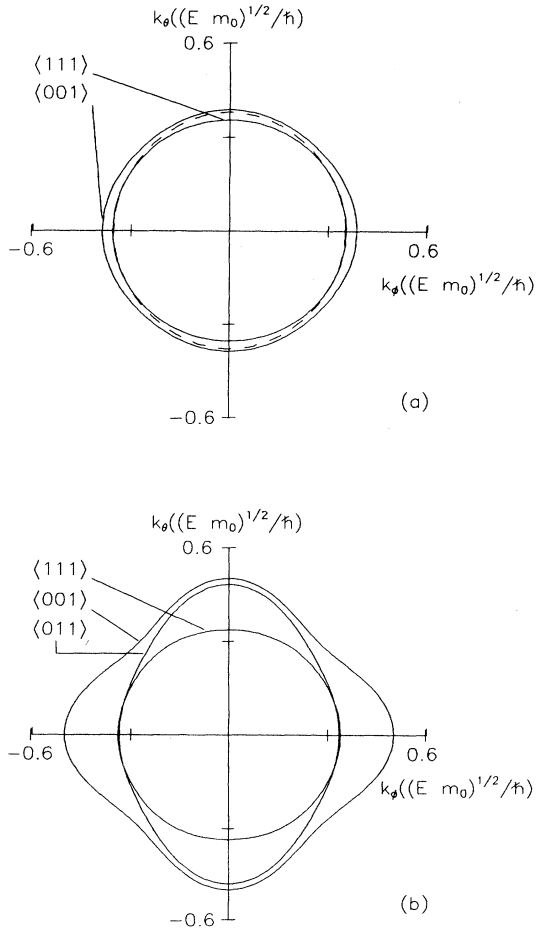

FIG. 8. Isoenergetic curves of ⟨001⟩-, ⟨011⟩-, and ⟨111⟩-oriented surface states; (a) HgTe, (b) α-Sn. In the isotropic approximation, γ_2 and γ_3 are replaced by $\gamma = (2\gamma_2 + 3\gamma_3)/5$.

V. CONCLUSIONS

We carried out systematic calculations of the valence-band structure for ⟨011⟩- and ⟨111⟩-oriented quantum wells, and found the nonparabolicity of the subbands. The orientation of the layer is found to be a key parameter in a 2D valence-band structure design. Going from ⟨001⟩ through ⟨011⟩ to ⟨111⟩ orientation, we can qualitatively change the dispersion of the first excited subband of cubic semiconductor layers according to the scheme: negative mass → saddle point → positive mass. This scheme is applicable also to gapless semiconductors, where, independent of the orientation, the ground hole subband has an electroniclike behavior. For gapless semiconductors, the gap appearing as a result of size quantization depends crucially on the layer orientation. Orientation is also found to be an important parameter in determining whether surface states do exist in the crystal, and their 2D dispersion.

The analytical dispersion relations found by us are generalized for strained layers. The influence and magnitude of the strain on the hole spectrum vary with the film orientation. Only in ⟨001⟩ layers, the applied strain results in a constant shift at $\boldsymbol{k}_{\parallel} = \mathbf{0}$ of the heavy subbands relative to the light subbands. The manifestation of the new dispersion features in such phenomena as cyclotron resonance and infrared absorption measurements are highlighted.

[1] E. P. O'Reilly, Semicond. Sci. Technol. **4**, 121 (1989).
[2] B. Laikhtman, R. A. Kiehl, and D. J. Frank, J. Appl. Phys. **70**, 1531 (1991).
[3] L. G. Gerchikov and A. V. Subashiev, Fiz. Tekh. Poluprovodn **25**, 231 (1991) [Sov. Phys. Semicond. **25**, 140 (1991)].
[4] J. H. Neave, J. Zhang, X. M. Zhang, P. M. Fawcett, and B. A. Joyce, Appl. Phys. Lett. **62**, 753 (1993).
[5] K. Inoue, K. Kimura, K. Maehashi, S. Hasegawa, H. Nakashima, M. Iwane, O. Matsuda, and K. Murase, J. Cryst. Growth **127**, 1041 (1993).
[6] A. V. Chaplik and L. D. Shvartsman, Sov. Phys. Surf. Phys. Chem. Mech. **2**, 73 (1982).
[7] S. S. Nedorezov, Fiz. Tverd. Tela **12**, 2269 (1970) [Sov. Phys. Solid State **12**, 1814 (1971)].
[8] M. I. D'yakonov and A. V. Khaetskii, Zh. Eksp. Teor. Fiz. **82**, 1584 (1982) [Sov. Phys. JETP **55**, 917 (1982)].
[9] L. D. Shvartsman, Solid State Commun. **46**, 787 (1983).
[10] O. V. Kibis and L. D. Shvartsman, Sov. Phys. Surf. Phys. Chem. Mech. **7**, 119 (1985).
[11] L. C. Andreani, A. Pasquarello, and F. Bassani, Phys. Rev. B **36**, 5887 (1987).
[12] Bradley A. Foreman, Phys. Rev. B **49**, 1757 (1993).
[13] D. A. Broido and L. J. Sham, Phys. Rev. B **31**, 888 (1985).
[14] G. D. Sanders and Y. C. Chang, Phys. Rev. B **32**, 4282 (1985).
[15] C. Y. P. Chao and S. L. Chuang, Phys. Rev. B **46**, 4110 (1992).
[16] J. M. Luttinger and W. Kohn, Phys. Rev. **97**, 869 (1955).
[17] J. N. Schulman and Y. C. Chang, Phys. Rev. B **33**, 2594 (1986).
[18] G. A. Baraff and D. Gershoni, Phys. Rev. B **43**, 4011 (1991).
[19] L. G. Gerchikov and A. V. Subashiev, Semiconductors **27**, 249 (1993).
[20] G. Shechter, L. D. Shvartsman, and J. E. Golub, J. Appl. Phys. (to be published).
[21] G. Harbeke, M. Cardona, and R. Blachnik, in *Physics of Group IV Elements and III-IV Compounds*, edited by O. Madelung, Landolt-Börnstein, New Series, Group III, Vol. 17, Pt. a (Springer, Berlin, 1982); G. Nimtz, in *Physics of II-VI and I-VII Compounds, Semimagnetic Semiconductors*, edited by O. Madelung, Landolt-Börnstein, New Series, Group III, Vol. 17, Pt. b (Springer, Berlin, 1982).
[22] R. Eppenga and M. F. H. Schuurmans, Phys. Rev. B **37**, 10 923 (1988).
[23] M. I. D'yakonov and A. V. Khaetskii, Zh. Eksp. Teor. Fiz. **33**, 115 (1981) [Sov. Phys. JETP **33**, 110 (1981)].
[24] G. C. Osbourn, J. Appl. Phys. **53**, 1586 (1982).
[25] G. L. Bir and G. E. Pikus, *Symmetry and Strain-Induced Effects in Semiconductors* (Wiley, New York, 1974).
[26] E. O. Kane, J. Phys. Chem. Solids **1**, 82 (1956).
[27] J. S. Park, R. P. G. Karunasiri, and K. L. Wang, Appl. Phys. Lett. **61**, 681 (1992).
[28] I. M. Tsidilkovskii, *Band Structure of Semiconductors*, 1st ed. (Oxford, New York, 1982).